JOURNAL OF AIRCRAFT
Vol. 38, No. 4, July–August 2001

Assessment of Flight Simulator Fidelity in Multiaxis Tasks Including Visual Cue Quality

R. A. Hess* and W. Siwakosit†
University of California, Davis, California 95616-5294

A technique for analytical assessment of flight simulator fidelity is presented as an extension of a methodology previously introduced in the literature. The assessment is based on a computer simulation of the pilot and vehicle and is inherently task dependent. A simple model of visual cue quality is introduced that is based on the classical concept of human operator visual remnant. The complete assessment procedure now includes proprioceptive, vestibular, and visual cue modeling. Inverse dynamic analysis is employed that allows the use of compensatory models of the human pilot in multiaxis tasks. The methodology is exercised by considering a simple rotorcraft lateral and vertical repositioning task in which visual and motion cue quality is varied.

Nomenclature

$[\boldsymbol{A}, \boldsymbol{B}, \boldsymbol{C}, \boldsymbol{D}]$	=	state-space quadruple defining closed-loop pilot/vehicle system
$[\boldsymbol{A}_G, \boldsymbol{B}_G, \boldsymbol{C}_G, \boldsymbol{D}_G]$	=	state-space quadruple defining inverse dynamics filter G
d_i	=	number of times expression for ith pilot/vehicle response variable must be differentiated for tracking command to appear explicitly
d var	=	parameter controlling multiplicative noise in visual cue model
$\boldsymbol{E}, \boldsymbol{F}$	=	matrices involved in definition of inverse dynamics system
$e^{-\tau_0 s}$	=	time delay in pilot model
$\boldsymbol{G}$	=	transfer function matrix defining inverse dynamics filter
$\boldsymbol{G}_D$	=	transfer function matrix describing pilot/vehicle response to tracking command inputs with inverse dynamic system
h	=	rotorcraft height in repositioning task, ft
h_{com}	=	rotorcraft height command, ft
h_e	=	rotorcraft heigth error, $h_c - h$, ft
$K_{\dot{m}}$	=	gain on structural model vestibular signal
$\boldsymbol{P}$	=	state-space quadruple $[\boldsymbol{A}, \boldsymbol{B}, \boldsymbol{C}, \boldsymbol{D}]$
q_i	=	polynomial whose reciprocal describes inverse dynamics between ith pilot/vehicle response variable and ith tracking command
ts	=	sampling period in visual cue model
$\boldsymbol{V}$	=	vector of input tracking commands in inverse dynamics system
Y_e	=	gain and low-frequency integration on structural model visual error signal
Y_{FS}	=	force-feel system dynamics in structural model of pilot
Y_{NM}	=	neuromuscular system dynamics in structural model of pilot
Y_{PF}	=	proprioceptive feedback dynamics in structural model of pilot
y	=	rotorcraft lateral displacement in repositioning task, ft
y_{com}	=	rotorcraft lateral displacement command, ft
y_e	=	rotorcraft lateral displacement error, $y_c - y$, ft
δ_A	=	lateral cyclic input measured at pilot's hand, in.
δ_C	=	collective input measured at pilot's hand, in.
ϕ	=	vehicle roll attitude, rad

Received 5 January 2001; presented as Paper 2001-4250 at the AIAA Modeling, Simulation, and Technology Conference, Montreal, Canada, 6–9 August 2001; revision received 10 April 2001; accepted for publication 11 April 2001.

*Professor and Vice-Chairman, Department of Mechanical and Aeronautical Engineering, One Shields Avenue; rahess@ucdavis.edu. Associate Fellow AIAA.

†Graduate Student, Department of Mechanical and Aeronautical Engineering; currently Lecturer, Department of Mechanical Engineering, Kasetsart University, Bankok 10900, Thailand.

Introduction

FLIGHT simulation facilities constitute an important tool for both pilot training and flight control research. The fidelity of the simulator is of prime importance in the successful use of these facilities. Here, simulation fidelity can be defined as "the degree to which characteristics of perceivable states induce adequate pilot psychomotor and cognitive behavior for a given task and environment."[1] Assessment of simulator fidelity is usually undertaken through subjective pilot fidelity ratings and comments, for example, Refs. 2 and 3. However, analytical approaches to fidelity assessment are also needed. The research summarized here builds on the analytical framework introduced and developed in Refs. 4–6. In particular, a mechanism for including visual cue quality is introduced with origins in the classical treatment of human operator remnant, for example, Ref. 7. Furthermore, well-developed compensatory tracking models of the human pilot behavior are utilized with the aid of an inverse dynamic analysis technique similar to that employed in Ref. 6, but now rendered computationally efficient.

The use of compensatory tracking models is not a minor issue. These models and their parameterization have been the subject of considerable research over the past four decades. With such models the analyst can predict the basic form of pilot equalization given the dynamics of the vehicle and a hypothesized manual feedback topology.[7,8] The primary drawback to the use of compensatory models arises in computer simulation of discrete tracking tasks such as those characterizing many low-altitude rotorcraft maneuvers. In such computer simulations, unrealistic control activity and vehicle angular velocities are typically predicted at maneuver initiation. This has led some researchers to propose dual-mode pilot models in which pilot dynamics are different at the beginning of a maneuver than at its conclusion.[9] Although such models possess a certain amount of face validity, their parameterization is difficult, especially if they are to be used in predictive fashion.

The procedure employed in Ref. 6 allowed the use of compensatory models by creating outer-loop position commands that produced desired pilot/vehicle trajectories in the tasks being studied. A technique for formalizing and automating this procedure is

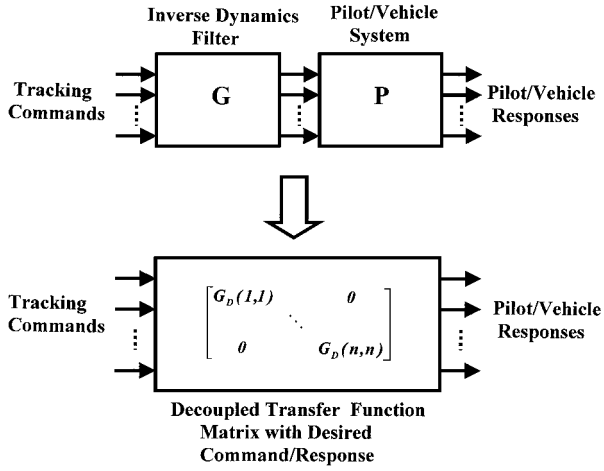

Fig. 1 Inverse dynamics analysis.

summarized in the following section, with a particular emphasis on multiaxis tasks.

Inverse Dynamic Analysis

Assume that a state-space model of the closed-loop, pilot/vehicle system has been obtained. This would be created using compensatory tracking models of the pilot in inner loops, with appropriate pilot compensation in outer loops. An example of doing this for a simple single-axis task is given in Ref. 6. The state-space quadruple for the closed-loop system can be given as

$$\boldsymbol{P} = [\boldsymbol{A}, \boldsymbol{B}, \boldsymbol{C}, \boldsymbol{D}] \tag{1}$$

Figure 1 shows the structure of the inverse dynamic system to be discussed. The filter matrix denoted $\boldsymbol{G}$ produces a decoupled system between the tracking commands and the pilot/vehicle system responses. The transfer function matrix between commands and responses can be represented by a diagonal matrix whose elements are simple, low-order transfer functions. By the use of a technique introduced in Ref. 10, a state-space quadruple $[\boldsymbol{A}_G, \boldsymbol{B}_G, \boldsymbol{C}_G, \boldsymbol{D}_G]$ of the filter matrix $\boldsymbol{G}$ can be obtained as

$$\boldsymbol{A}_G = \left(\boldsymbol{A} - \boldsymbol{B}\boldsymbol{E}_R^{-1}\right), \qquad \boldsymbol{B}_G = \boldsymbol{B}\boldsymbol{E}_R^{-1}$$

$$\boldsymbol{C}_G = -\boldsymbol{E}_R^{-1}\boldsymbol{F}, \qquad \boldsymbol{D}_G = \boldsymbol{E}_R^{-1} \tag{2}$$

where $\boldsymbol{E}_R^{-1}$ is the right inverse of the matrix $\boldsymbol{E}$. Matrices $\boldsymbol{E}$ and $\boldsymbol{F}$ are defined as

$$\boldsymbol{E}_i = a_{i0}\boldsymbol{C}_i\boldsymbol{A}^{(d_i-1)}\boldsymbol{B}, \qquad \boldsymbol{F}_i = \sum_{j=0}^{d_i} a_{ij}\boldsymbol{C}_i\boldsymbol{A}^{(d_i-j)} \tag{3}$$

where d_i is the number of times one has to differentiate the expression for the ith vehicle response before a tracking command explicitly appears. The vector expression for the vehicle responses $\boldsymbol{Y}(s)$ to the vector expression for tracking commands $\boldsymbol{V}(s)$ can be given by

$$\boldsymbol{Y}(s) = \text{diag}[1/q_i(s)]\boldsymbol{V}(s) \tag{4}$$

where

$$q_i(s) = a_{i0}s^{d_i} + a_{i1}s^{(d_i-1)} + \cdots + a_{ij}s^{(d_i-j)} + \cdots + a_{id_i} \tag{5}$$

and the polynomial $q_i(s)$ is selected by the analyst, that is, once the value of d_i is obtained for each tracking command/response pair, the coefficients of $q_i(s)$ can be selected. Thus, for example, the (decoupled) transfer function between pilot/vehicle response $y_i(s)$ and tracking command $v_i(s)$ is given by

$$y_i(s) = [1/q_i(s)]v_i(s) \tag{6}$$

The mechanism that provides the tracking/response relations such as that in Eq. (6) is the filter transfer function matrix $\boldsymbol{G}$, whose realization as a transfer function matrix can be obtained from the state-space quadruple of Eq. (2). The process just described has been automated in a MATLAB® M-file. To obtain the final diagonal transfer function matrix with elements approximating unity, the ith tracking command must be multiplied by $q_i(s)$ with the final elements having been made proper by the addition of an appropriate number of stable, high-frequency poles. As a final note, the difficulties associated with applying dynamic inversion to systems with nonminimum phase dynamics pose no problems here. The unstable poles appearing in $\boldsymbol{G}$ are replaced by their mirror images with respect to the imaginary axis. The resulting phase errors in the elements of $\boldsymbol{G}$ are minimized in the frequency range of interest for manual control (0.1–10 rad/s) by time delays on the desired inputs.

Modeling Visual Cue Quality

Model

The model for visual cue quality is based on the classical concept of human operator remnant and was developed with an eye toward efficient computer simulation of the resulting pilot/vehicle system. Thus, it was desired to minimize model parameterization while still allowing the resulting structure to produce effective remnant spectral characteristics that approximated those resulting from classical human-in-the-loop tracking experiments, and that produced effects in human operator dynamic characteristics similar to those obtained in experiment, for example, Ref. 11.

Reference 12 surveyed pertinent literature regarding the effects of variation in display quality on measured human operator describing functions in laboratory tracking tasks. Citing six studies (Refs. 11, 13–17), it was shown that reduction in display quality of various types resulted in 1) an increase in the effective time delay in the human operator describing function and 2) an increase in tracking error in the task(s) at hand. Reference 12 demonstrated that the increase in time delay could be attributed to a gain reduction in the propriopceptive feedback used by the human operator, that is, the delay increase may not be associated with the visual process, per se. However, it was felt that a baseline delay increase associated with the visual process when using degraded displays would be a reasonable modeling assumption. With this in mind, the two operations considered to be essential to a visual cue model were 1) sampling and 2) noise corruption.

Periodic sampling (with a zero-order hold) is capable of producing an increase in effective time delay approximately equal to half the sampling interval,[18] whereas noise corruption is capable of increasing tracking error. The model itself is intended to capture the effects of visual information display in a control theoretic context and, as such, represents the interface between the display medium and the resulting stimuli to the human pilot. Figure 2 compares a single-axis tracking task employing the injected-error remnant with the tracking structure using a serial visual cue model. The visual cue model is shown separately to distinguish it from the transfer function representation of the pilot. The relatively simple visual cue model that included these operations and that was capable of closely approximating measured remnant spectral characteristics is shown in Fig. 3.

In the model of Fig. 3, the displayed error, denoted as model input, is fed through a sample and hold element, with the sampling period

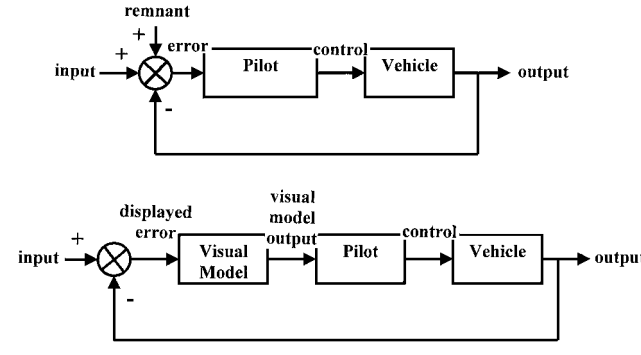

Fig. 2 Comparison of injected-remnant tracking structure with visual cue model structure.

ts. As Fig. 2 indicates, the resulting discrete signal is multiplied by a magnitude-limited random number, with variance d_{var}, and is then filtered. The resulting filtered signal is added to the output of the sample and hold element to produce the model output.

Comparison with Classical Remnant Models

A computer simulation of a compensatory tracking task was created with the human operator represented by the structural model of the human pilot.[6] Two sets of vehicle dynamics were chosen, $1/s$ and $1/s^2$. The visual model sampling period *ts* was chosen to provide a sampling frequency approximately 50 times the closed-loop pilot/vehicle bandwidth, which is approximately 2 rad/s. Thus,

$$ts = 2\pi/2.50 = 0.0628\,\text{s} \approx 0.06\,\text{s} \tag{7}$$

The variance *d*var was then selected as that which scaled the resulting effective remnant power spectral density (PSD) so that acceptable matches to measured remnant PSDs reported in the literature could be obtained. The effective remnant was created as the random signal that reproduced the output of the visual cue model when added to the displayed error. Figure 4 shows a portion of the visual model input and output time histories in the computer simulation of the pilot/vehicle system with $1/s$ vehicle dynamics. The tracking command was a random signal. Figures 5 and 6 compare the PSDs of these effective remnant signals with those from Ref. 11 for the two-vehicle dynamics. Note that the magnitudes of the PSDs are calculated as $10\log_{10}|\cdot|$. Acceptable matches are seen to result. Note specifically that the PSD of the effective remnant scales with the mean square value of the displayed error just as the case with the experimental results of Ref. 11. Figure 7 shows the effect of varying *d*var on the PSD of the effective remnant. The parameter *d*var is thus seen to play a role similar to the noise–signal ratio of injected observation noise in algorithmic models of the human operator such as the optimal control model.[8]

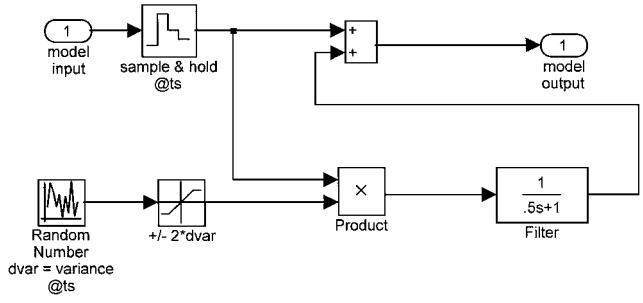

Fig. 3 Visual cue model.

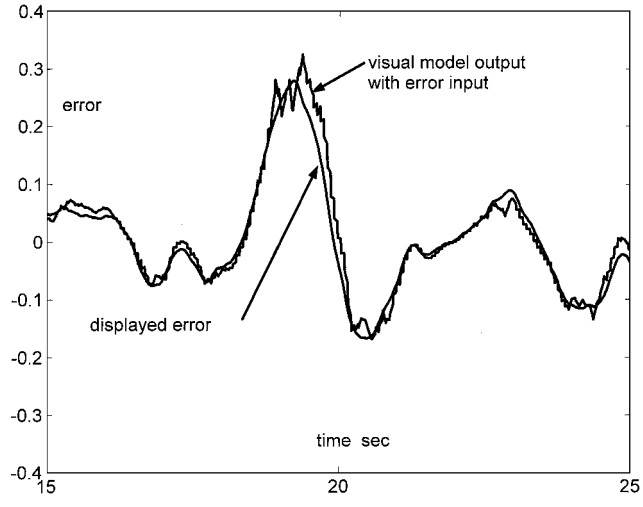

Fig. 4 Visual model input–output time histories.

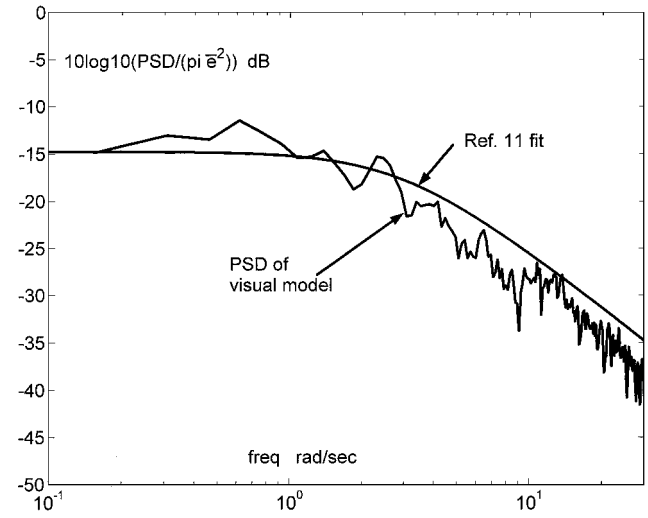

Fig. 5 Comparison of PSD of effective remnant from visual cue model with that from experiment; vehicle dynamics = $1/s$.

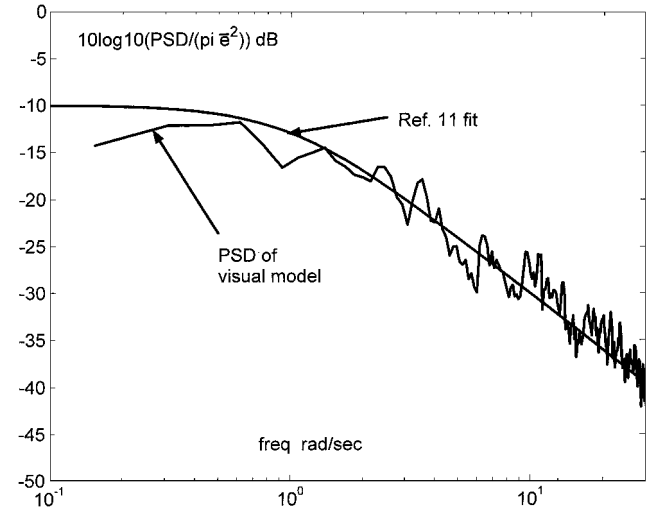

Fig. 6 Comparison of the PSD of effective remnant from visual cue model with that from experiment; vehicle dynamics = $1/s^2$.

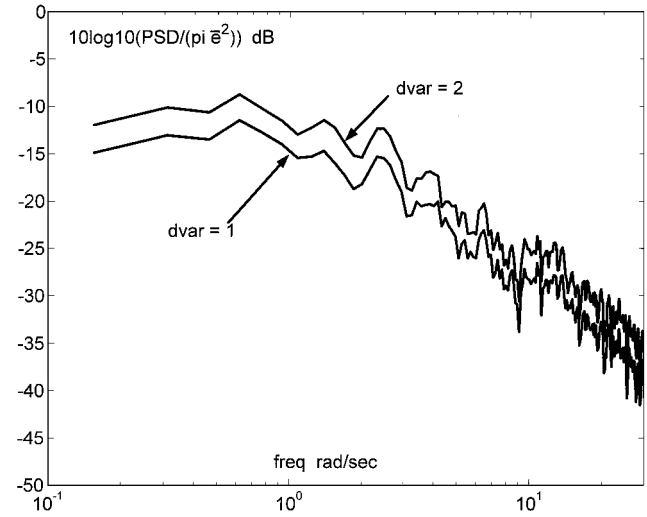

Fig. 7 PSD of effective remnant from visual cue model for different values of *d*var.

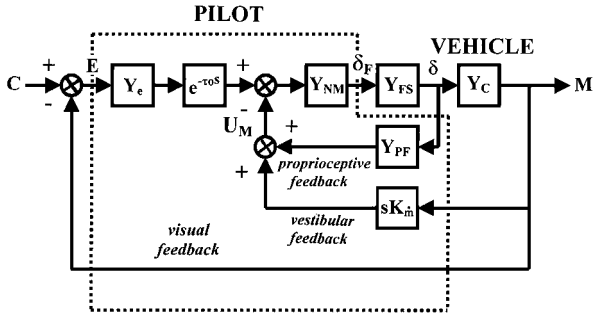

Fig. 8 Structural model of the human pilot.

Fidelity Assessment with the Structural Pilot Model

Analytical assessment or prediction of simulator fidelity is undertaken in exactly the same manner as discussed in Ref. 6. The handling qualities sensitivity function (HQSF) is the magnitude of a transfer function derived from the structural model of the human pilot that is shown in single-axis form in Fig. 8. The HQSF is defined as

$$\text{HQSF} = |U_M/C(j\omega)| \tag{8}$$

A MATLAB-based computer-aided design package referred to as PVD_{NL} is utilized in creating the pilot model and in calculating the HQSF that is plotted vs ω on linear scales.[19] As discussed in Ref. 6, a fidelity metric can be defined using the differences in areas beneath the HQSF curves for a nominal vehicle and the vehicle as simulated across all inner-loop axes being controlled by the pilot. Hence,

$$\text{fidelity metric} = \frac{1}{n}\sum_{i=1}^{n}\left[\frac{\Delta\text{area}}{\text{normalizing area}}\right]_i \tag{9}$$

where n is the total number of inner-loop axes being controlled by the pilot, i refers to the ith axis of control, and Δ area refers to the area between the HQSF curve for the nominal or flight vehicle and that for the vehicle as being simulated, and normalizing area refers to the area beneath the HQSF for the nominal or flight vehicle.

The larger the value of the metric defined by Eq. (9), the poorer is the predicted simulator fidelity. In both area calculations just defined, the pilot model parameters are based on the nominal vehicle and left unchanged when the simulated vehicle is analyzed via computer simulation.

Example

Nominal Vehicle and Pilot Models

At this juncture, a simple example of the assessment technique described in the preceding sections is in order. The vehicle model is a linear, simplified version of the hover dynamics of an unaugmented BO-105 rotorcraft as taken from Ref. 20. The vehicle dynamics are

$$\begin{Bmatrix}\dot{w}\\ \dot{v}\\ \dot{p}\\ \dot{\phi}\end{Bmatrix} = \begin{bmatrix}0 & 0 & 0 & 0\\ 0 & -0.036 & -1.76 & 32.2\\ 0 & -0.063 & -9.91 & 0\\ 0 & 0 & 1 & 0\end{bmatrix}\begin{Bmatrix}w\\ v\\ p\\ \phi\end{Bmatrix}$$

$$+\begin{bmatrix}-11.1 & 0.0086\\ -0.059 & 0.807\\ -0.13 & 2.8\\ 0 & 0\end{bmatrix}\begin{Bmatrix}\delta_C\\ \delta_A\end{Bmatrix}$$

The amount of coupling between vertical and lateral axes is quite small in this model and is created by off-axis control inputs. Table 1 gives the dynamics of the two motion systems to be compared in the analysis. They have been categorized as large-motion and small-motion systems as described in Ref. 21. The large-motion system is comparable to the NASA Ames Research Center vertical motion simulator (VMS), whereas the small-motion system is representative of hexapod motion devices.

Table 1 Motion system definitions

Axis	Large motion	Small motion
Vertical	$0.8(0)^2/[0.707,0.3]$[a]	$0.13(0)^2/[0.707,0.9]$
Lateral	$0.5(0)^2/[0.707,0.5]$	$0.45(0)^2/[0.707,0.9]$
Roll	$0.4(0)^2/[0.707,0.5]$	$0.25(0)/(0.81)$

[a]Equal to $0.8s^2/[s^2 + 2(0.707)(0.3)s + (0.3)^2]$.

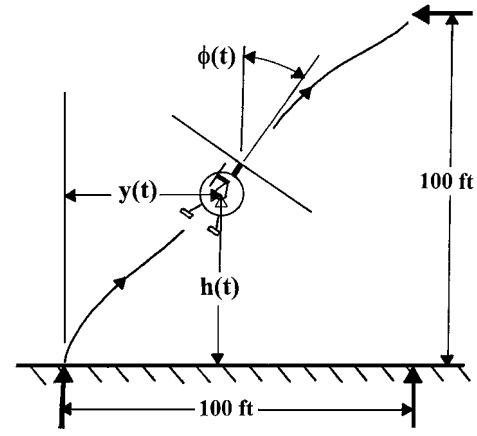

Fig. 9 Hover lateral and vertical repositioning task.

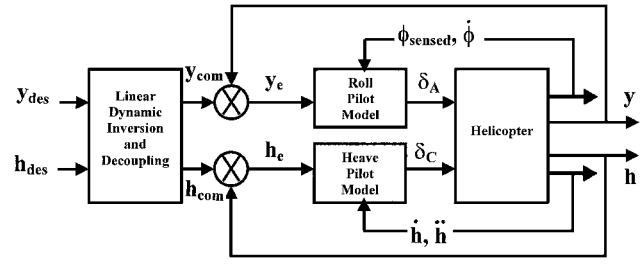

Fig. 10 Pilot/vehicle system for the task of Fig. 9.

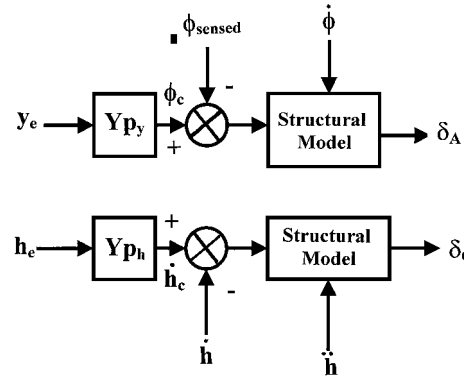

Fig. 11 Pilot models of Fig. 10.

The flight task is shown in Fig. 9 and represents a 100-ft lateral and vertical repositioning task initiated and completed in a condition of stabilized hover. Figure 10 is a block diagram of the pilot/vehicle system to be modeled. For the sake of clarity, the visual cue model and motion system dynamics have been omitted. Figure 11 shows the pilot model blocks of Fig. 10 in more detail. The inclusion of ϕ_{sensed} in the inner-feedback roll-attitude loop in Fig. 10 deserves some comment. The vestibular feedback implicit in the structural model of Fig. 8 derives from the study in Ref. 22. There it was

Table 2 Pilot model parameters

Elements	Values
Inner-loop	
Common	
τ_0	0.2
Y_{NM}	100/[0.707,10]
Roll axis	
Y_e	22.95(0.4)/(0)
Y_{FS}	625/[0.707,25]
$K_{\dot{m}}$	3.11
Heave axis	
Y_e	0.829
T_{FS}	10/(0)(10)
$K_{\dot{m}}$	0.13
Outer-loop	
Lateral axis, $\phi_c/y_e = Yp_y$	0.238(0.2)/(10)
Heave axis, $\dot{h}_c/h_e = Y_{p_h}$	1.0

demonstrated that inclusion of a feedback loop involving the first derivative of the inner-loop vehicle response variable being controlled by the pilot could explain measured human pilot dynamic characteristics when motion cues were present. The utility of outer-loop motion quantities such as lateral acceleration could not, however, be directly explained by this model. Here it is hypothesized that lateral acceleration can serve as a surrogate cue for roll attitude, thus reducing the visual workload associated with the roll-axis task. This surrogate cue was blended with the visually sensed roll attitude as follows:

$$\phi_{\mathrm{sensed}} = 0.75\phi_{\mathrm{visual}} + 0.25(1/32.2)\ddot{y} \tag{10}$$

where ϕ_{sensed} is an output from the visual model. The four-to-one variation in gain values in Eq. (10), is of course, conjecture. However, the impact of this assumption on fidelity assessment is mitigated by the gain values remaining invariant in the analysis to follow.

The structural model parameters resulting from application of $\mathrm{PVD_{NL}}$ for the inner loops controlling vehicle roll and heave are given in Table 2. The pilot outer-loop compensation elements Yp_y and Yp_ϕ are also given in Table 2 along with the dynamics of the force-feel systems in the cyclic and collective cockpit inceptors. The inner- and outer-loop crossover frequencies for each axis were selected as 2 and 1 rad/s, respectively.

Visual cue models were employed in the input channel for each structural model inner-visual loop of Fig. 10, that is, ϕ_e and $\dot{h}_e$. In the outer visual loops, visual cue models were employed in the error channels for each variable created by the outer-loop compensation. For example, consider the compensation for the outer-loop element of the lateral axis given in Table 2 where an $(s + 0.2)$ factor appears in numerator of the ϕ_c/y_e transfer function. This implies that in creating ϕ_c, the pilot employs an internally generated signal proportional to $y_e(t) + 0.2\dot{y}_e(t)$. In simulating the pilot/vehicle system, separate visual cue models were employed for $y_e(t)$ and $\dot{y}_e(t)$.

The command trajectories for the lateral and vertical repositioning task were identical and were given by

$$y_{\mathrm{des}}(t) = h_{\mathrm{des}}(t) = \tfrac{100}{16}[\cos(3 \cdot \pi \cdot t/10) - 9\cos(\pi \cdot t/10) + 8]\,\mathrm{ft} \tag{11}$$

The visual model parameters for the nominal or flight vehicle are given in the third and fourth columns of the first row of Table 3. Note that the parameter $d$var is a factor of 10 smaller than the value used in obtaining the PSD plots of Figs. 5 and 6. The reason for using this smaller value is that five visually sensed variables are involved in the rotorcraft simulation, that is, ϕ_e, y_e, $\dot{y}_e$, h_e and $\dot{h}_e$, whereas only a single variable was involved in the computer simulation of the single-axis task that yielded Figs. 5 and 6. Selection of $d\mathrm{var} = 0.1$ was somewhat arbitrary and based on obtaining stable simulations with realistic pilot control inputs. Also note that, for simplicity and

Table 3 Configuration definitions

Configuration	Motion	$d$var	ts, s	del m, s	del v, s	Fidelity metric
Nominal	Perfect	0.1	0.06	0	0	0
1	Large	0.1	0.06	0.05	0.05	0.21
2	Small	0.1	0.06	0.05	0.05	0.47
3	Large	0.25	0.06	0.05	0.05	0.28
4	Small	0.25	0.06	0.05	0.05	0.53
5	Large	0.1/0.25[a]	0.06	0.05	0.05	0.30
6	Small	0.1/0.25	0.06	0.05	0.05	0.47
7	Large	0.1	0.06	0.025	0.075	0.24
8	Large	0.1	0.06	0.075	0.025	0.25
9	Large	0.1	0.06	0.035	0.1	Unstable
10	Large	0.1	0.06	0.1	0.035	0.29
11	Large	0.1	0.06	0.045	0.125	Unstable
12	Large	0.1	0.06	0.125	0.045	0.28
13	Static	0.1	0.06	N/A	0.05	Unstable

[a]Here 0.1 on position variables, 0.25 on rate variables.

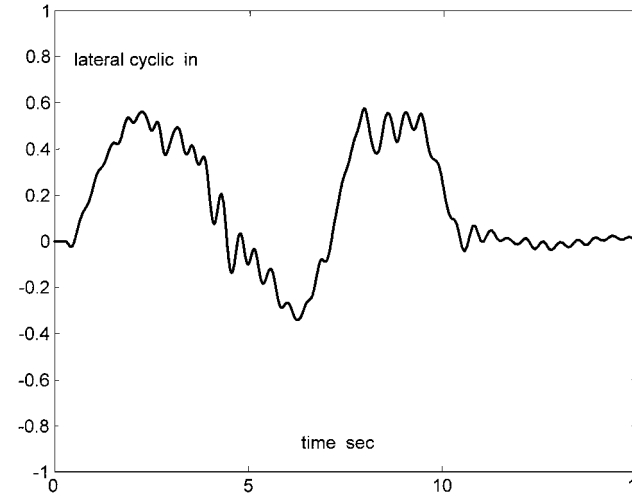

Fig. 12 Lateral cyclic control input from computer simulation with nominal pilot/vehicle system.

with the exception of translational rate cues $\dot{h}_e$ and $\dot{y}_e$ in configurations 5 and 6, the same value of $d$var was used in all of the visual models.

Figures 12 and 13 show the lateral cyclic and collective commands from the pilot models when the commands of Eq. (11) were applied to the system of Fig. 10. These time histories are qualitatively similar to those obtained in flight test or pilot-in-the-loop simulation, that is, the fundamental waveforms appear as one or two period sinusoids corrupted by noise. Figure 14 shows the vehicle lateral response. The heave or vertical response was nearly identical to that shown in Fig. 14.

Figures 15 and 16 show the HQSFs from the roll and heave inner-loop structural pilot models. The HQSFs for cases with and without the visual model are shown in each Figs. 15 and 16 for the sake of comparison. The jagged appearance of the HQSFs for the cases when the visual model is in place is a result of the noise injection and limiting that occurs within the visual model, as indicated in Fig. 3.

Varying Simulation Parameters

Table 3 shows 13 configurations representing conditions that could lead to reduction of simulator fidelity. The fifth and sixth columns represent time delays that may accrue in the motion del m and visual del v systems. The conditions represented in Table 3 involve variation in motion dynamics (large vs small-motion systems and motion time delays), visual cue quality ($d$var), and temporal mismatches between motion and visual cues (unequal del m and del v values).

As an example of the area calculations called out in Eq. (9), Fig. 17 shows the normalizing area for the roll-axis structural model HQSF

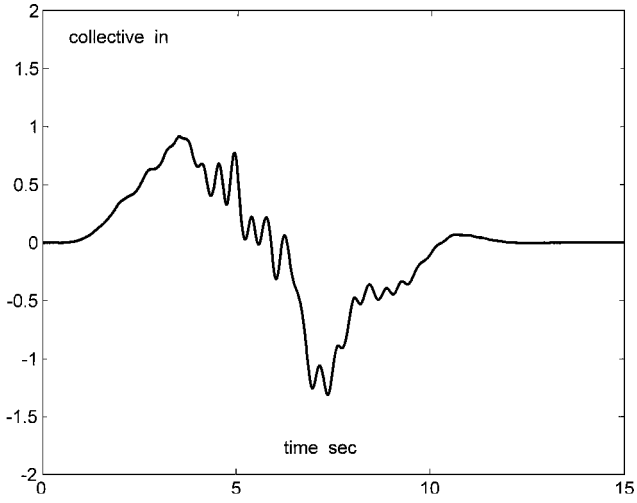

Fig. 13 Collective control input from computer simulation with nominal pilot/vehicle system.

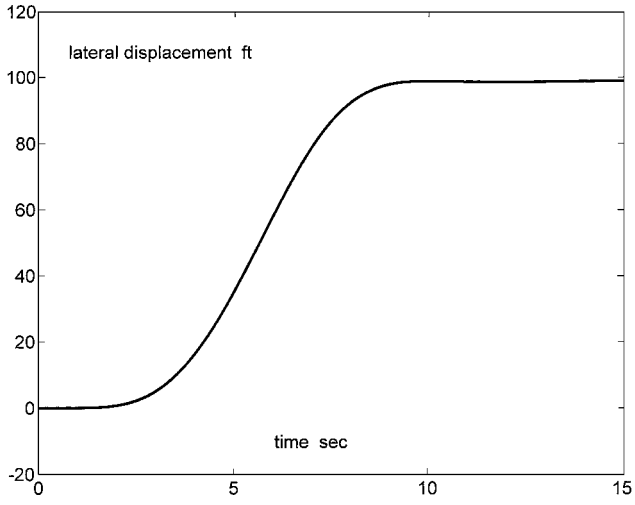

Fig. 14 Lateral response time history from computer simulation with nominal pilot/vehicle system.

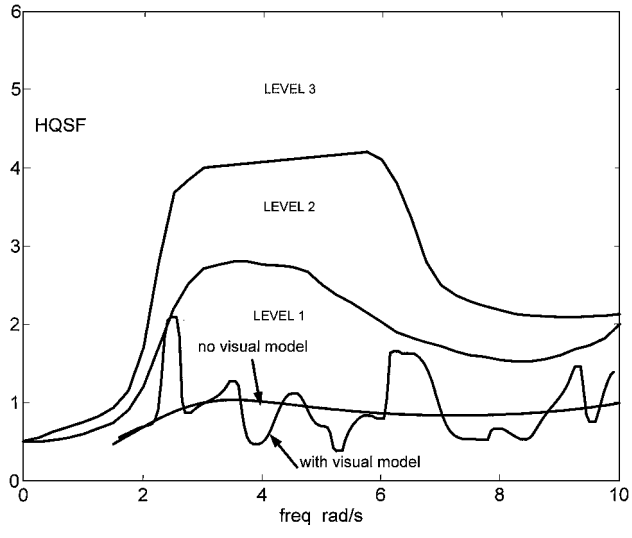

Fig. 15 HQSFs for roll-axis structural model.

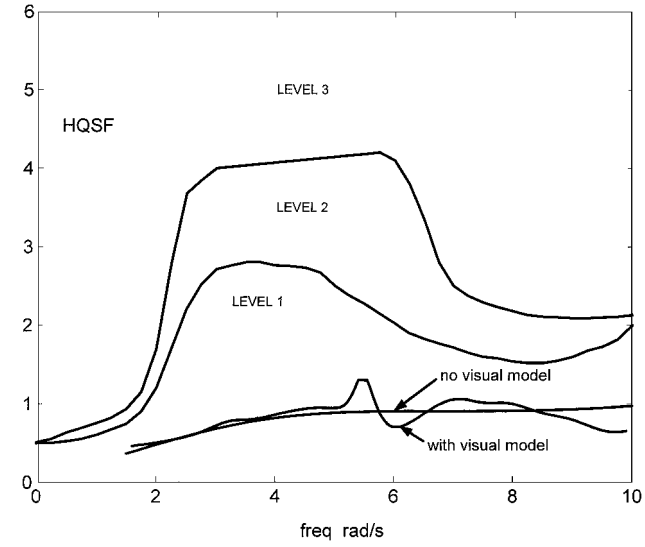

Fig. 16 HQSFs for heave-axis structural model.

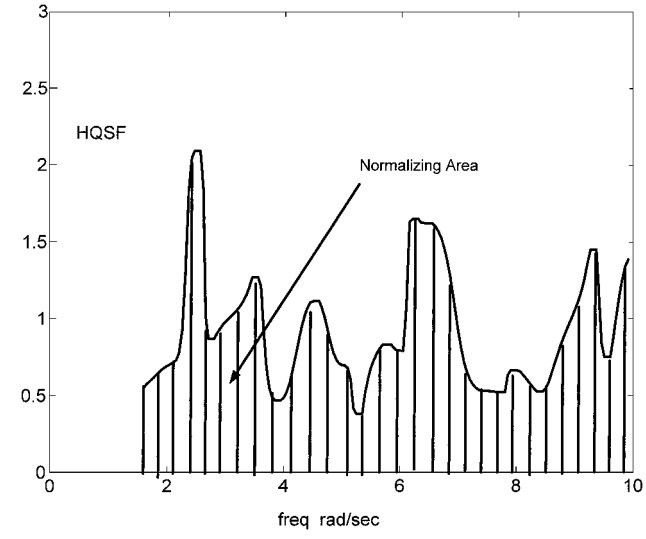

Fig. 17 Normalizing area for roll-axis structural model HQSF.

and Fig. 18 shows the Δ area for the heave-axis HQSFs between the nominal heave configuration and that of configuration 1 in Table 3. The final column of Table 3 tabulates the value of the fidelity metric defined by Eq. (9). As Table 3 indicates, the computer simulation of the pilot/vehicle system was unstable in three cases. This does not imply that the actual piloted simulation would be unstable. Recall that the fidelity assessment procedure freezes the pilot model parameters at values appropriate to the nominal or flight vehicle (Table 2) and then applies this model in a computer simulation of the system with simulator limitations.

Figures 19 and 20 graphically compare the fidelity metrics for 12 of the 13 configurations of Table 3. These comparisons predict that, for this task, large-motion systems will exhibit higher fidelity than small-motion systems in spite of differences in visual cue quality (Fig. 19) and that in cases of temporal mismatches between motion and visual cues, the visual should lead the motion (Fig. 20). The contraindication of this last conclusion for configurations 7 and 8 in Fig. 20 is quite small, and the differences noted are probably within the model's margin of error. Also note in Table 3 that the static or no-motion condition was unstable, indicating poor fidelity. Finally, a comparison of the fidelity metrics for configurations 1 and 2 and 3 and 4 would suggest that motion system characteristics dominate visual system characteristics.

The results just summarized offer few surprises. Indeed, the configurations of Table 3 were deliberately chosen to allow the

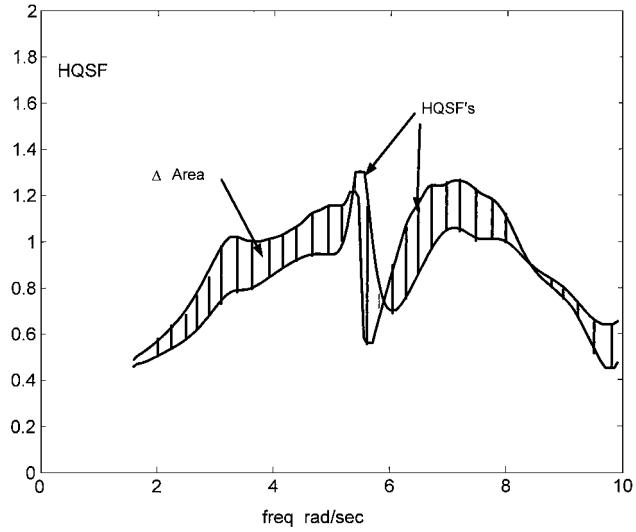

Fig. 18 Δ area for heave-axis HQSFs between nominal heave configuration and that of configuration 1 in Table 3.

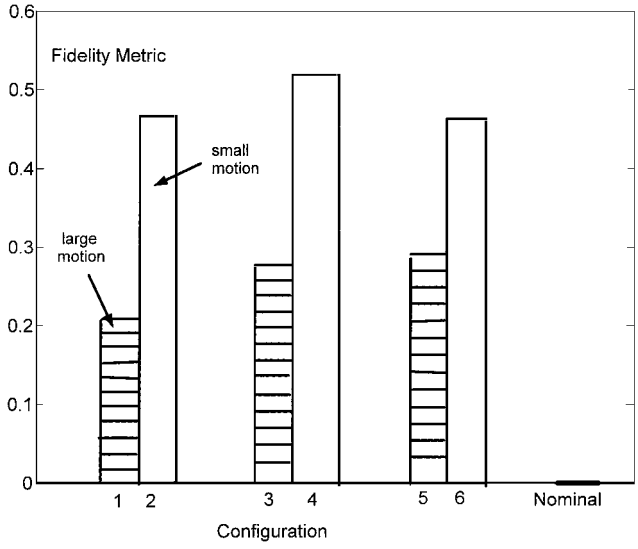

Fig. 19 Comparison of fidelity metrics for configurations 1–6 and nominal configuration of Table 3.

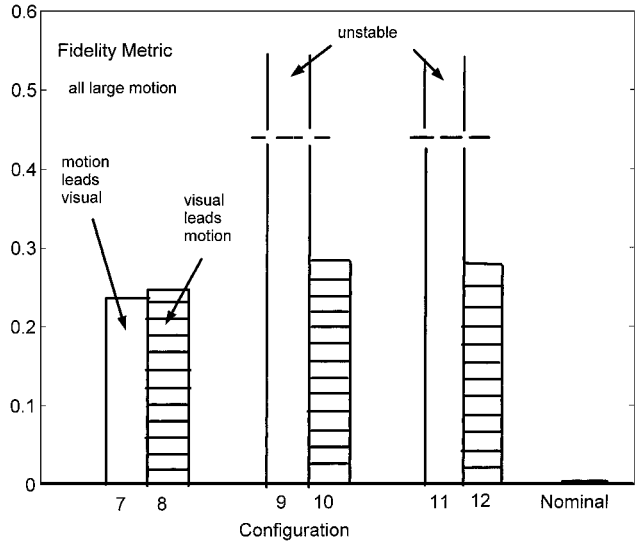

Fig. 20 Comparison of fidelity metrics for configurations 7–12 and nominal configuration of Table 3.

analytical approach to quantify results that have been experimentally verified, albeit with vehicles and tasks differing in detail from those studied here. Reference 21 demonstrated the superiority of large-motion systems as compared to small or no-motion (static) systems. Reference 23 indicated that visual cues should be synchronous with motion cues, or at worst, the visual cues should lead the motion cues. Finally, Ref. 3 demonstrated that motion system dynamics had a considerable stronger effect upon fidelity ratings than did variations in visual scene characteristics.

Model Deficiencies

The model for assessing flight simulator fidelity discussed herein is not without deficiencies, and two are immediately apparent. First, a means of correlating a given visual scene representation in a simulator to a specific set of *d*var or *ts* values is yet to be established. Second, a means of correlating the value of the fidelity metric of Eq. (9) with subjective measures of simulator fidelity is needed. The former deficiency is shared with most, if not all, control theoretic representations of human pilot behavior, although some progress has been made in this area in terms of the optimal control model of the human pilot, for example, Ref. 24. The latter deficiency is less formidable and can be attacked by comparing values of the fidelity metric with subjective measures of simulation fidelity in analyzing the results of pilot-in-the-loop simulations reported in the literature, for example Refs. 21 and 23.

Conclusions

A methodology for the analytical assessment of flight simulator fidelity previously introduced in the literature has been extended to include a measure of visual cue quality. The methodology thus includes the effects of proprioceptive, vestibular, and visual cues. In addition, inverse dynamics analysis allows the use of well-established, compensatory models of human pilot behavior, now extended to multiaxis tasks. Fidelity assessment is based on a metric derived from pilot-model-based HQSF. Exercise of the methodology on a simple example of a rotorcraft lateral and vertical repositioning maneuver indicated that fidelity assessments could be derived that were consonant with experimental results obtained in pilot-in-the-loop simulation studies.

Acknowledgements

This research was supported by Cooperative Research Agreement NCC2-5369 with NASA Ames Research Center. The Grant Technical Manager was Duc Tran.

References

[1] "Proposed Study of Simulation Validation/Fidelity for NASA Simulators," Ad Hoc Advisory Subcommittee on Avionics, Controls, and Human Factors, List of Definitions, Committee Tasks, and Study Scope, NASA, Nov. 1979.

[2] Schroeder, J. A., "Evaluation of Simulation Motion Fidelity Criteria in the Vertical and Directional Axes," *Journal of the American Helicopter Society*, Vol. 41, No. 2, 1996, pp. 44–57.

[3] Schroeder, J. A., Chung, W. W. Y., and Hess, R. A., "Evaluation of Motion Fidelity Criterion with Visual Scene Changes," *Journal of Aircraft*, Vol. 37, No. 4, 2000, pp. 580–587.

[4] Hess, R. A., and Malsbury, T., "Closed-Loop Assessment of Flight Simulator Fidelity," *Journal of Guidance, Control, and Dynamics*, Vol. 14, No. 1, 1991, pp. 191–197.

[5] Hess, R. A., Malsbury, T., and Atencio, A., Jr., "Flight Simulator Fidelity Assessment in a Rotorcraft Lateral Translation Maneuver," *Journal of Guidance, Control, and Dynamics*, Vol. 16, No. 1, 1993, pp. 79–85.

[6] Zeyada, Y., and Hess, R. A., "Human Pilot Cue Utilization with Applications to Simulator Fidelity Assessment," *Journal of Aircraft*, Vol. 37, No. 4, 2000, pp. 588–597.

[7] McRuer, D. T., and Krendel, E. S., "Mathematical Models of Human Pilot Behavior," AGARDograph 188, 1974.

[8] Hess, R. A., "Feedback Control Models–Manual Control and Tracking," *Handbook of Human Factors and Ergonomics*, edited by G. Salvendy, 2nd ed., Wiley, New York, 1997, Chap. 38.

[9] Ferguson, S. W., Clement, W. F., Cleveland, W. B., and Key, D. L., "Assessment of Simulation Fidelity Using Measurements of Piloting Technique in Flight," American Helicopter Society, Paper A-84-08-4000, May 1984.

[10]Snell, S. A., "Decoupling Control Designs with Applications to Flight," *Journal of Guidance, Control, and Dynamics*, Vol. 21, No. 4, 1998, pp. 647–655.

[11]Jex, H. R., Allen, R. W., and Magdaleno, R. E., "Display Format Effects on Precision Tracking Performance, Describing Functions, and Remnant," Aerospace Medical Research Lab., AMRL-TR-71-63, Wright–Patterson AFB, OH, Aug. 1971.

[12]Hess, R. A., "Modeling the Effects of Display Quality upon Human Pilot Dynamics and Perceived Handling Qualities," *IEEE Transactions on Systems, Man, and Cybernetics*, Vol. 25, No. 2, 1995, pp. 338–344.

[13]Allen, R. W., Clement, W. F., and Jex, H. R., "Research on Display Scanning, Sampling, and Reconstruction Using Separate Main and Secondary Tracking Tasks," NASA CR-1569, 1970.

[14]Levison, W. H., Elkind, J. I., and Ward, J. L., "Studies of Multivariable Manual Control Systems: A Model for Task Interference," NASA CR-1746, May 1971.

[15]Hess, R. A., and Teichgraber, W. M., "Error Quantization Effects in Compensatory Tracking Tasks," *IEEE Transactions on Systems, Man, and Cybernetics*, Vol. SMC-4, No. 4, 1974, pp. 343–349.

[16]Zacharias, G. L., and Levison, W. H., "A Performance Analyzer for Identifying Changes in Human Operator Tracking Strategies," *Proceedings of the Fifteenth Annual Conference on Manual Control*, Univ. of Michigan, Ann Arbor, MI, Air Force Flight Dynamics Lab., AFFDL-TR-79-3134, 1979, pp. 187–211.

[17]Kenyon, R. V., and Kneller, E. W., "The Effects of Field-of-View Size on the Control of Roll Motion," *IEEE Transactions on Systems, Man, and Cybernetics*, Vol. 23, No. 1, 1993, pp. 183–193.

[18]Franklin, G. F., Powell, J. D., and Workman, M L., *Digital Control of Dynamic Systems*, 2nd ed., 1990, Addison Wesley Longman, Reading, MA, p. 119.

[19]Zeyada, Y., and Hess, R. A., "PVD_{NL}, Pilot/Vehicle Dynamics $_{Nonlinear}$, An Interactive Computer Program for Modeling the Human Pilot In Single-Axis Linear and Nonlinear Tracking Tasks," Dept. of Mechanical and Aeronautical Engineering, Univ. of California, Davis, CA, 1998.

[20]Heffley, R. K., Jewell, W. F., Lehman, J. M., and Van Winkle, R. A., "A Compilation and Analysis of Helicopter Handling Qualities Data, Vol. One: Data Compilation," NASA CR-3144, March 1979.

[21]Schroeder, J. A., Chung, W. W. Y., Tran, D. T., Laforce, S., and Bengford, N. J., "Pilot-Induced Oscillation Prediction with Three Levels of Simulation Motion Displacement," AIAA Paper 98-4333, Aug. 1998.

[22]Hess, R. A., "Model for Human Use of Motion Cues in Vehicular Control," *Journal of Guidance, Control, and Dynamics*, Vol. 13, No. 3, 1990, pp. 476–482.

[23]Chung, W. W. Y., Schroeder, J. A., and Johnson, W. W., "Effects of Vehicle Bandwidth and Visual Spatial-Frequency on Simulation Cueing Synchronization Requirements," AIAA Paper 97-3655, Aug. 1997.

[24]Wewerinke, P. H., "A Theoretical and Experimental Analysis of the Outside World Perception Process," *Proceedings of the Fourteenth Annual Conference on Manual Control*, Univ. of Southern California, Los Angeles, CP-2000, NASA, 1978, pp. 535–556.